

## Augmentation of Thermo-physical Properties of Porous Polymer Composite Film by Sonication

Debashis Panda<sup>1</sup>, Sanjay Kumar Rout<sup>2\*</sup> and Payodhar Padhi<sup>1</sup>

<sup>1</sup>Research and Development Center, Hi-Tech Medical College and Hospital, Bhubaneswar, Odisha, India

<sup>2</sup>Department of Chemistry, Konark Institute of Science and Technology, Bhubaneswar, Odisha, India

### Research Article

Received: 01/03/2018

Accepted: 28/03/2018

Published: 07/04/2018

#### \*For Correspondence

Sanjay Kumar Rout, Department of Chemistry, Konark Institute of Science and Technology, Techno Park, Jatni, Odisha, India, Tel: + 09438453824.

**Email:** sanjay.tulu@gmail.com

**Keywords:** Activated carbon, Uniformity, sonication, LLDPE, DTA, TGA, Porous polymer composite film

#### ABSTRACT

The systematic experimental design was pertained to optimize the effects of the concentration of activated carbon, on the thermo-physical properties (porosity, thermal degradation) of Porous Polymer Composite Film (PPCF). In this study, Linear Low-Density Polyethylene (LLDPE) of roto and film grade was used for synthesizing PPCF via cavitation-assisted solidification route with varying wt% of Activated Carbon (AC) in the polymer matrix. The cavitation effect was given by a water bath sonicator subjected to a particular frequency and sonication time. The fabricated flat sheet PPCF was characterized by using Field Emission Scanning Electron Microscope (FESEM), Differential Thermal Analysis (DTA), Thermo Gravimetric analysis (TGA) and Brunauer–Emmett–Teller (BET) analysis to establish a correlation between the filler concentration and their structural, morphological and thermal attributes. Among two different grade matrix materials (roto and film), roto grade LLDPE is unsuitable for PPCF making since it shows agglomerations, whereas low activated carbon concentration (5 wt%) shows a better result in film grade with conformal coverage. The activation energy decreases with increasing filler concentration. Sonication helps in de-agglomeration, uniform dispersion of the filler in matrices with reduction of mean pore diameter of LLDPEF 2.2 and LLDPER 2.2 from 0.26  $\mu\text{m}$  to 0.15  $\mu\text{m}$  (42.3%) and 1.02  $\mu\text{m}$  to 0.54  $\mu\text{m}$  (47.05%) along with enhancement in porosity by 48.5% and 13.84% respectively. Apart from gas separation/sensing, catalysis, energy storage, photonics, these fabricated PPCF can be used as micro-perforated sound absorption panel.

#### INTRODUCTION

Porous Polymer Composite Films (PPCF) have drawn extensive attention in recent years due to their unique and diversified applications in various fields such as photonics, gas separation/sensing, catalysis, energy storage, biomedical and tissue engineering [1-3]. In particular, porous polymer composite film consisting carbonaceous filler such as activated carbon, graphene and carbon nanotube have enormous utilities due to their thermo-chemical stability, superior chemical resistance and excellent thermal/electrical conductivity [4-7]. Various fabrication techniques such as phase separation, direct foaming, emulsion templating, polymer foam replication, immersion precipitation, vortex method, dip coating and solidification processing have been developed for porous polymer film [8-10]. "Breath figures" is another well-known method to fabricate porous polymer film by condensation of water vapour on the surface of organic polymer solvent solution [11]. Usually, immersion precipitation method used for preparing organic porous polymer membrane. However, during the fabrication process, these methods required precise control over the processing environment. Sometimes these methods are not economically suitable [12]. Teng et al. [8] fabricated porous polymer composite films by use of chloroform solution of poly (3-hexylthiophene) (P3HT) and (6,6)-phenyl-C61-butiric acid-methyl-ester (PCBM) via the freeze-drying method to study its wettability and adhesion behavior. Kuo et al. [13] synthesized porous polystyrene/poly (vinyl pyrrolidone) (PS/PVP) films, via phase separation in a dip-coating process, for anti reflection applications. Morita et al. [14] fabricated a porous composite membrane by the combination of polypyrrole (PPy) powder with a porous polypropylene film, which could be used to control ionic permeability. The desired property of any porous polymer composite film or any composite

structure depends upon the various factors such as filler concentration, uniformity in dispersion, surface energy and of course its porosity. A quite descriptive indeed review papers are available in open literature which focuses on synthesis and utilization of polymer matrix composite in various applications including mechanical, electrical, medical etc. [15-17]. It is worth noticing that the control of the compatibility between the two polymer phase and uniform dispersion of the filler in the matrix is quite difficult in chemical synthesis, especially in solution processing method [18]. In fact, the most important parameter for any polymer matrix composite is the combination of optimum surface tension with a maximum dispersion of separated particles [15]. Due to inter-particle Van der Waals force induced in filler/polymer solution, the agglomeration of filler material in the matrix is quite often. Consequently, the dispersion of agglomerated particle in the liquid media will require ample force to break the bond between the particles. In general, agitation found to be best suitable for better dispersion of the filler in the matrix. Agitation is provided by shear mixing, reflux, magnetic stirring or most commonly ultrasonication [19-22]. Researchers also try to improve the adhesion of the interface between the filler and matrix introducing functional group into the surface of filler (eg.  $\text{NH}_2$  group) or surfactant-treatment or by plasma treatment [16,23]. Yang et al. [21] found that ultrasonic wave might be the efficacious solution to counteract the problem of agglomeration. Transient acoustic cavitation and acoustic streaming are responsible for refining microstructure, degassing of liquid solvent and well dispersion of filler material in the matrix. During cavitation, the sound wave propagates through the liquid media via generating alternating high-pressure (compression) and low-pressure (rarefaction). In low-pressure cycle nucleation bubble initiated, gain its maximum size and then collapse violently during the high-pressure cycle. As a result, shock wave generates whose peak speed helps to break the agglomeration and distract the interparticle Van der Waals bond [19]. In polymeric phase, cavitation cause intensified polymerization or depolymerization reaction via dispersion of aggregates or permanent break down of the chemical bond [24,25]. Moreover, it is also observed that cavitation helps in the increasing the permeability of porous membrane because of bulk mass transfer during vibration of the membrane in any fluid media [26,27]. Ham et al. [12] use simple facile sonication method to fabricate macro porous polymer thin film from the temporarily stabilized water-in-oil emulsion. Lee et al. [28] reported that pore size of the film could be controlled by simply altering the concentration of the precursor solution along with the polymer chain lengths on the surfaces of the substrate. By increasing the concentration of polystyrene-grafted Graphene Oxide dispersion, they were able to decrease the pore size of the film from 4 to 1  $\mu\text{m}$ . Overvelde et al. [29] tailoring the pore shape of elastomeric structure (soft silicone based rubber) with theoretical and experimental means to achieve the desired mechanical properties such as lateral contraction and compaction by the development of new class of soft, active and reconfigurable device over a wide range of length scale. The author has reported that smaller values of porosity in the structure will responsible for macroscopic instability results limited compaction and higher values of porosity makes the material fragile during mechanical loading. Apart from mechanical and electrical application, PPCF has been used as sound absorbing material. When acoustic pressure wave i.e., called sound wave interact on a solid structure, it dissipates the energy through flexing of the solid frame. If the solid surface is non-porous, incident energy reflects back to the environment and get lost. However, porosity in the material increases the number of total internal reflection leads to huge energy losses due to friction and material suitable for absorbing source [30]. In fact, open and through pores are more helpful in sound absorbing in these material. Henceforth, porous material has been received huge attention as a sound absorber due to presence of cavities/channel/interstices. Recent studies majorly focus on varying the morphological properties of the material such as polyurethane and foams to enhance the acoustic performances (e.g., vibration and acoustic attenuations) [31,32]. Yang et al. [33] correlated the sound absorbing properties of the multilayered viscoelastic composites with different interface shapes. Arenas et al. [34] reported that micro-perforated panels are used as best sound absorbing materials now a days due to their uniform perforation, which enables sufficient friction between moving air molecules and the internal pore surface, owing to conversion of acoustical energy to heat. Sakagami et al. [35] did an experimental study on different micro-perforated panel absorbers with varies size of perforation to find the best sound absorber value. However, to the best of our knowledge, there are few studies has been done on utilization of the hydrophobic facile LLDPE porous polymer composite film as micro-perforated panels sound absorbers [34].

The present study is based on a communication of new methodology; the technique adopted here is very simple and eco-friendly. This is cleaner approach as the process does not pollute the environment and involves no toxic discharge; further Porous Polymer Composite Film (PPCF) was fabricated economically for different technical applications. Future aspects of this study can include proper utilization of polyethylene and carbon black (the environmental wastes by-product) for the fabrication of different types of PPCF, which may play a key role in the solid waste management of the environment for the benefit of society. In this work, Linear Low-Density Polyethylene (LLDPE) of film grade as well as roto grade is chosen as matrix and activated carbon of different weight% used as filler during synthesis of porous polymer composite films. The current experiment establishes a correlation between the filler concentration with the structural, morphological and thermal aspects of PPCF and explicates the effect of sonication on porosity development. Although the acoustic absorption experiment has not been done, our results provide the sufficient validation for the applicability of fabricated PPCF possibly as sound absorption material for developing micro-perforated sound absorbers panel.

**Table 1.** Filler Fraction (wt%) in LLDPE PPCF (film grade and roto grade).

Sample Code	Wt of Filler (in g)	Wt of Polyethylene (in g)	Filler fraction (In average wt%)
LDPE (F/R) 2.2	0.2	2	5
LDPE (F/R) 2.3	0.3	2	10
LDPE (F/R) 3.2	0.2	3	15

<sup>F</sup> Film grade, <sup>R</sup> Roto grade

## MATERIALS AND METHODS

### Materials

Linear Low-Density Polyethylene (LLDPE) film grade (density=0.918 g/cc) and roto grades (density=0.946 g/cc) were kindly provided by Central Institute of Plastics Engineering and Technology (CIPET) Bhubaneswar, Odisha, India used as a continuous phase. Commercial Activated carbon (AC) of Darco type was selected as inorganic filler purchased from Sigma Aldrich (purity >99%). Phenol was purchased from Fisher Scientific UK Ltd; used as a solvent. Ultrasonic bath (Bandelin-Germany Make- Model: RK-100H) used as an ultrasonic generator to produce an ultrasonic frequency of 35 kHz. The homemade rectangular Pyrex glass molds (dimension=100 × 50 mm<sup>2</sup>) along with film casting knife are used for the preparation of film.

### Fabrication of porous polymer composite films

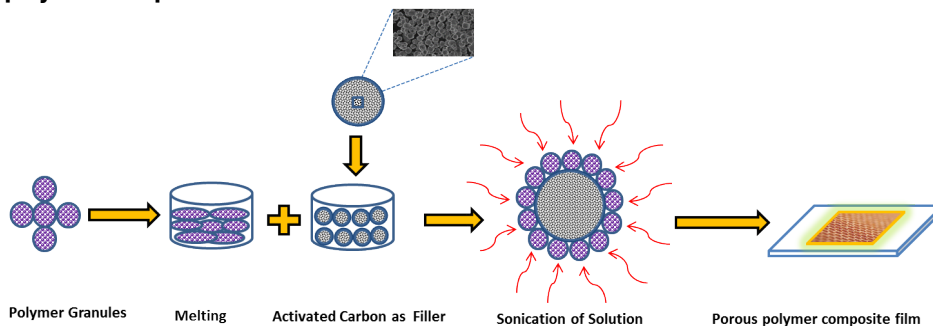


**Figure 1.** Schematic illustration of preparation of PPCF.

**Figure 1,** shows the schematic diagram of preparation of PPCF. The details procedure is given below.

- 2 g of LLDPE granules of different grades (film and roto) was melted in an oven at 120 °C/min for 1 h. In order to remove the moisture content, the filler material (AC) was dehydrated at a temperature about 130 °C/min in a vacuum oven for a period of 8 h.

- The different wt% (5%, 10%, and 15%) of activated carbon (filler fraction) was mixed in the 20 mL of phenol (solvent) in a 100 mL beaker. The composition of all suspensions is expressed by considering a weight percentage (wt%) of the AC filler with respect to the total solute mass (filler+ matrix) are listed in **Table 1**. The weight% calculation AC is mentioned in equation.1

$$\text{Filler fraction} = \frac{(\text{weight of the filler})}{(\text{weight of the filler}) + (\text{weight of the polymer})} \times 100 \tag{1}$$

- Subsequently, vigorous stirring of melted polymer along with a mixture of AC and phenol followed by ultrasonic dispersion was carried out in a water bath sonicator for 0.5 h. The sonication was done in hot condition (average temperature 120 °C).

- Then the hot solution was poured into the glass mold followed by flattening with the help of casting knife. The casted film was dried at room temperature about 6h. Later the resulting film was subjected to calcination up to temperature 130 °C for 3 h in an inert atmosphere with a slow heating rate (1 °C/min).

- The PPCF fabricated by LLDPE of film grade and roto grade was denoted as LLDPEF and LLDPER respectively.

### Characterization

The textural properties (surface area, pore volume, pore size) of the filler (AC) were determined using Quantachrome Autosorb iQ<sub>2</sub> automated gas sorption system. The surface morphology and the compositions of the PPCF were examined using field emission scanning electron microscope equipped with energy dispersive X-ray spectroscopy (FESEM model ZEISS EM910) operated at a voltage of 15 kV.

The thermogravimetric study (TGA) was done to analyze the thermal stability and degradation behavior of PPCF using Mettler-

Toledo TGA/SDTA851 thermal analyzer. Samples were transferred to TG pan and were heated in room temperature to 800 °C at a heating rate 5 °C/min . The amount of weight loss and the rate of weight loss (dTG=dW/dT) at corresponding temperatures were recorded.

The pore size distribution of the PPCF before and after cavitation was examined through careful analysis of microscopic image via ImageJ free software.

## RESULTS AND DISCUSSION

### Textural Characterization of the Activated Carbon Filler

The activated carbon powder samples are evacuated for 8 h at a temperature of 130 °C prior to N<sub>2</sub> adsorption, whereas N<sub>2</sub> adsorption was measured at -196.15 °C. Brunauer–Emmett–Teller (BET) surface areas are calculated using data obtained from adsorption in a relative pressure (p/p<sub>0</sub>) ranging from 0.05 to 0.30. In addition to above, the pore size is estimated using Non-Local Density Functional Theory (NLDFT) and pore volume is calculated from the amount of adsorbed N<sub>2</sub> at p/p<sub>0</sub>=0.99 using single point adsorption method respectively. **Table 2** represents the physicochemical properties of the filler material. The pore size of the activated carbon belongs to the mesoporous range. It is quite clear that high surface area activated carbon is suitable for PPCF making.

**Table 2.** Physicochemical properties of Activated carbon.

Sample	Surface area (m <sup>2</sup> g <sup>-1</sup> )	Pore volume (cm <sup>3</sup> g <sup>-1</sup> )	Pore size (Å)
Darco	979	0.51	21.01

### FESEM of PPCF

The surface and cross-sectional FESEM images of the LLDPEPPCF of film and roto grade before and after sonication are shown in **Figures 2a-2f, 2a<sub>1</sub>-2f<sub>1</sub> and 3a-3f, 3a<sub>1</sub>-3f<sub>1</sub>** respectively. The images are taken at a nominal magnification in range 15K to 80K. It is clear that 5% filler addition in LLDPE of film grade shows the homogeneous distribution of carbon in LLDPE support as compared to higher wt% (10, 15). However, with the increase in filler concentration, the rate of agglomeration effect increases in both film grade and roto grade. Moreover, the agglomeration effect is well significant in roto grade as compared to film grade as indicated from **Figure 3c-3f**. As sonication strongly affected by its peak power and amount of sample, the shock wave generates during sonication can easily propagate through the low-density liquid as compared to higher one. Hence lesser weight of the sample (weight of AC + weight of LLDPE) shows pronounces conformal coverage as compared to higher weight <sup>[19,36]</sup>. In addition to de-agglomeration, sonication helps to increase the mobility of pores, henceforth bigger pore diminishes and new continuous smaller pore generates, which happens due to increase in porosity. The large pore generated in PPCF might be the junction of several cracks or due to collapse of air bubble during calcination <sup>[37]</sup>. It can be seen that the large rift present at a cross-section of LLDPEF 2.2 before sonication becomes disappear after 0.5 h sonication and smaller thread like pore generate (**Figure 2b<sub>1</sub> and 2d<sub>1</sub>**), which have a stronger impact on augmenting permeability and porosity. The effect of ultrasonic cavitation on small pore formation in LLDPEF 2.2 PPCF is represented in **Figure 2a, 2b, 2a<sub>1</sub> and 2b<sub>1</sub>** respectively.

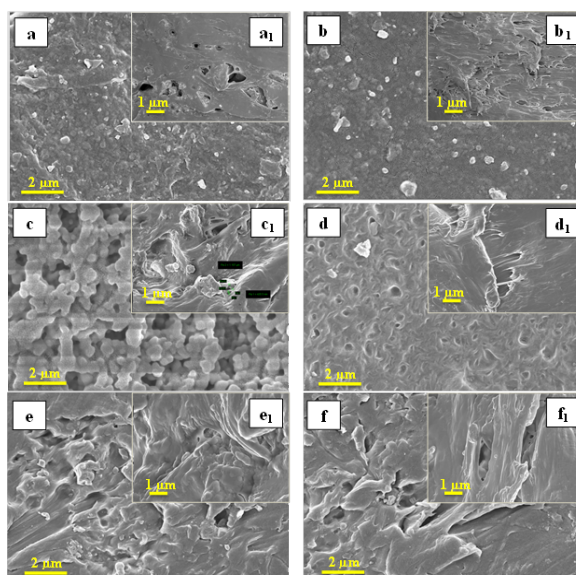


**Figure 2.** FESEM surface images of LLDPE film grade PPCF before (left) and after (right) sonication with inserted cross-sectional images: (a,b) surface images of LLDPEF 2.2 and (a<sub>1</sub>,b<sub>1</sub>) corresponding cross-sectional images; (c,d) surface images of LLDPEF 2.3 and (c<sub>1</sub>,d<sub>1</sub>) corresponding cross-sectional images; (e,f) surface images of LLDPEF 3.2 and (e<sub>1</sub>,f<sub>1</sub>) corresponding cross-sectional images.

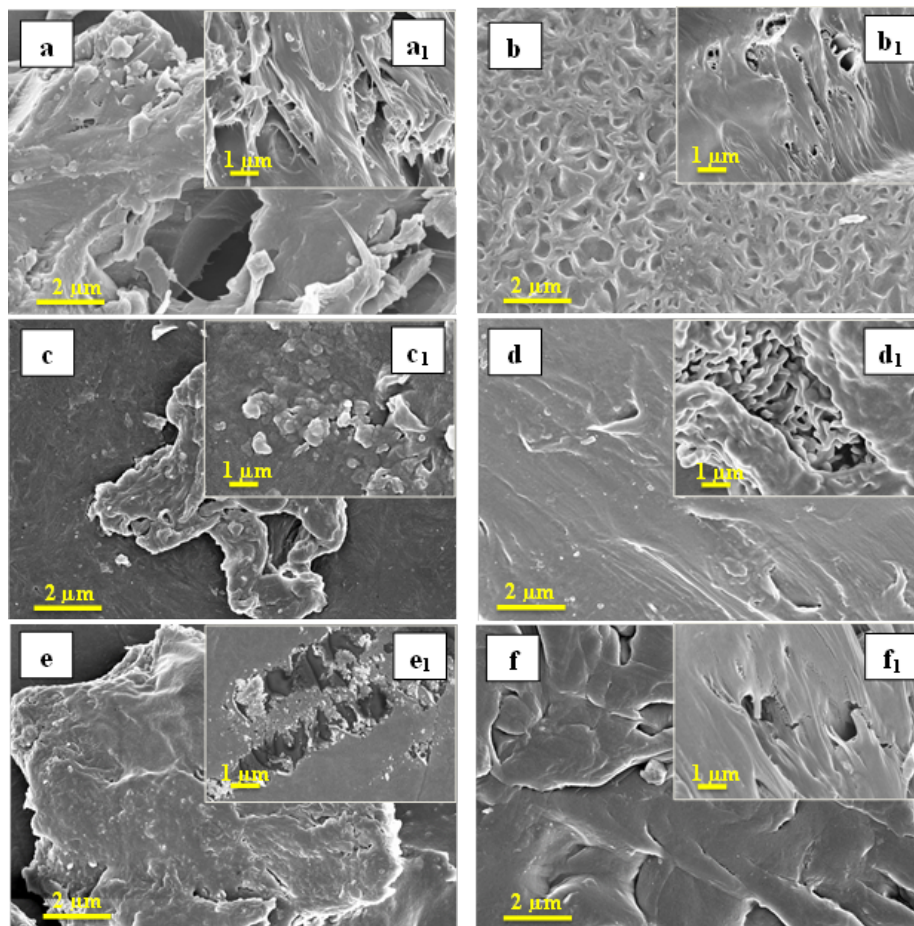


**Figure 3.** FESEM surface images of LLDPE roto grade PPCF before (left) and after (right) sonication with inserted cross-sectional images: (a,b) surface images of LLDPER 2.2 and (a<sub>1</sub>,b<sub>1</sub>) corresponding cross-sectional images; (c,d) surface images of LLDPER 2.3 and (c<sub>1</sub>,d<sub>1</sub>) corresponding cross-sectional images; (e,f) surface images of LLDPER 3.2 and (e<sub>1</sub>,f<sub>1</sub>) corresponding cross-sectional images.

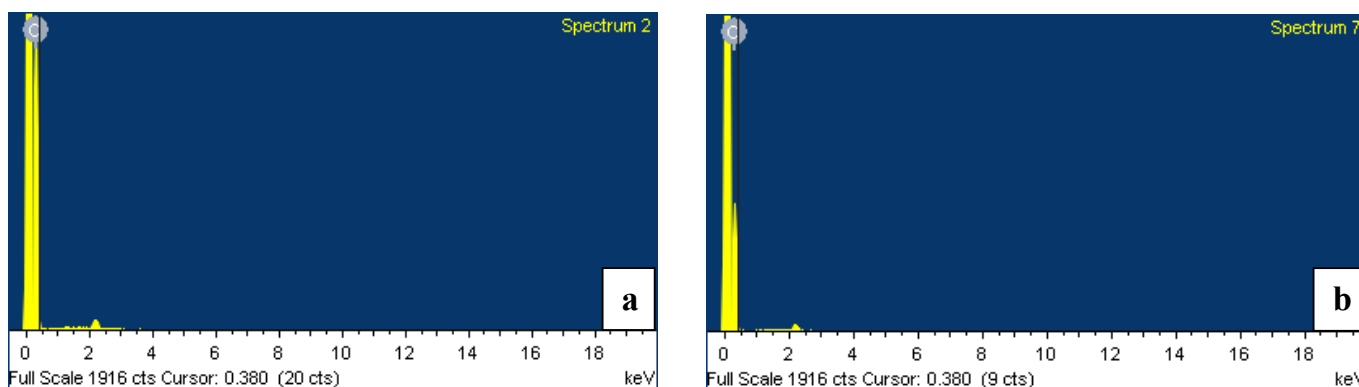


**Figure 4.** Selected EDS of (a) LLDPEF 2.2 before sonication and (b) LLDPEF 2.2 after sonication.

Similarly, Energy Dispersive X-ray Spectroscopy (EDS) was done for qualitative comparison to reveal any change in elemental compositions of the PPCF before and after sonication. As the carbon is the major element of the PPCF, the peak intensity of the signal corresponds to carbon, does not vary before and after sonication which is clearly indicated from **Figure 4a and 4b** respectively.

**Pore Size Distribution of PPCF**

The statistical pore size distribution used to explicate the pore density, porosity and the nucleation of the new pores in the homogeneous area of the PPCF before and after the 0.5 h of sonication. The pore size distribution analysis mainly considers the “homogeneous” parts of the PPCF surface, which does not exhibit larger pore or any cracks. The pore is assumed to be circular and isolated from each other. The edge dislocation effect is neglected. The pore density is calculated by dividing the

number of labeled pores per unit area, whereas the porosity is the total porous surface divided by total area of the image of the corresponding film. The calculated pore frequency is intended as the ratio of the number of pores with the pore radius between  $r$  and  $r+i$  (where  $i=0.5 \mu\text{m}$  is an interim gap between pore) to the total numbers of the pore. The theoretical calculation of the pore attribute is reported earlier [37]. The variation in pore-size is primarily due to the nature of frothing as well as the possibility of bubble coalescence [38]. The pore density, porosity and mean pore diameter for the two types of PPCF (LLDPEF 2.2, LLDPER 2.2) before and after sonication are given in **Table 3**.

**Table 3.** Pore size distribution of PPCF (LLDPEF 2.2 and LLDPER 2.2).

	LLDPEF 2.2		LLDPER 2.2	
	Before	After	Before	After
Pore Density ( $10^4 \text{ m}^{-2}$ )	$0.053 \pm 0.30$	$0.064 \pm 0.20$	$0.013 \pm 0.50$	$0.060 \pm 0.80$
Mean pore diameter ( $\mu\text{m}$ )	$0.26 \pm 0.27$	$0.15 \pm 0.11$	$1.02 \pm 1.13$	$0.54 \pm 0.21$
Porosity (%)	$7.79 \pm 0.15$	$11.57 \pm 0.20$	$9.03 \pm 0.20$	$10.28 \pm 0.60$

All the parameters are deduced from microscopic image processed through ImageJ software

Selected areas of focus in both of these films are almost similar. It is clear that after sonication, the mean pore diameter decreases for both cases in between 40-50%; nevertheless, there is an increase in pore density and porosity up to 17-83% due to the generation of numbers of small pores. These variations indicate the nature of porosity after cavitation in both of these films. Moreover, in order to epitomize the amount of pores formation, the graph is plotted between the relative frequency and pore diameter which is represented in **Figure 5**. The pore size distribution is greatly affected by the cavitation. In both LLDPEF 2.2 and LLDPER 2.2, the larger pores lying between 0.5 and 1.2  $\mu\text{m}$  in diameter get reduced to 0.15  $\mu\text{m}$  and 0.54  $\mu\text{m}$  respectively. As a result, the uniformity of the smaller pore (size varying between  $0.05 \approx 1 \mu\text{m}$ ) becomes more frequent in both of the cases. However, the result is more pronounced in film grade as compared to roto grade. This indicates due to cavitation effect, the nucleation of new smaller pores likely to generate more in composite possessing lesser molecular weight. The hydrodynamic cavitation has a significant role in decreasing pore size and even particle size which is previously reported by many researchers [39-41]. The pore size reduction and augmentation of porosity are quite comparable to other studies listed in **Table 4**.

**Table 4.** Comparison of porosity of various porous polymer composite films.

Composite	Fabrication method	Pore size reduction (%)	Porosity (%)	Method of calculation	References
PVA/MWCNT+MnO <sub>2</sub>	SP and ES	13.37	-	SEM	42
PMMA/MWCNT	NIPS	-	$37.30 \pm 0.3$	WE	43
PVDF/CNT	Breath-figure	67.44	-	SEM	28
PS/GO	SP	-	86.8-92.6	Fraction	38
LLDPE/AC	SP	42.30	$11.57 \pm 0.20$	SEM	This study

PVA: Poly vinyl alcohol, MWCNT: Multi wall carbon nano tube, PMMA: Poly (methyl methacrylate), PVDF: Poly (vinylidene fluoride), PS: Polystyrene, GO: Graphene Oxide, LLDPE: LinearLow-Density Polyethylene, SP: Solution Processing, ES: Electro Spinning, NIPS: Non-solvent induced phase separation, SEM: Scanning Electron Microscope, WE: Water Evaporation method.

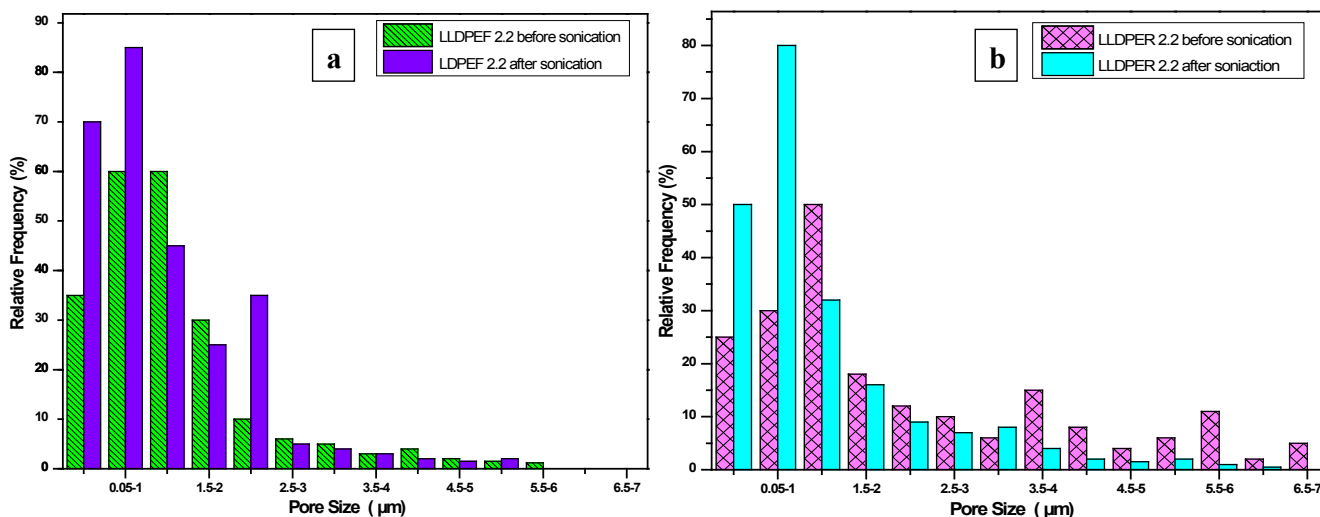


**Figure 5.** Pore size distribution ( $\mu\text{m}$ ) of (a) LLDPEF 2.2 and (b) LLDPER 2.2 before and after sonication.

**Thermogravimetric Analysis of PPCF**

Thermogravimetric analysis is one of the widely used techniques in the study of thermal properties of the PPCF which deliver the necessary information about the thermal stability along with the kinetic parameter subjected to decomposition process [42-44]. To investigate the thermal stability of different PPCF named as LLDPEF 2.2, LLDPEF 2.3, LLDPEF 3.2 and LLDPER 2.2 respectively, TGA test is done at a heating rate of 10 °C/min under an N<sub>2</sub> atmosphere from 25-1000 °C on different sample having masses of 12 mg.

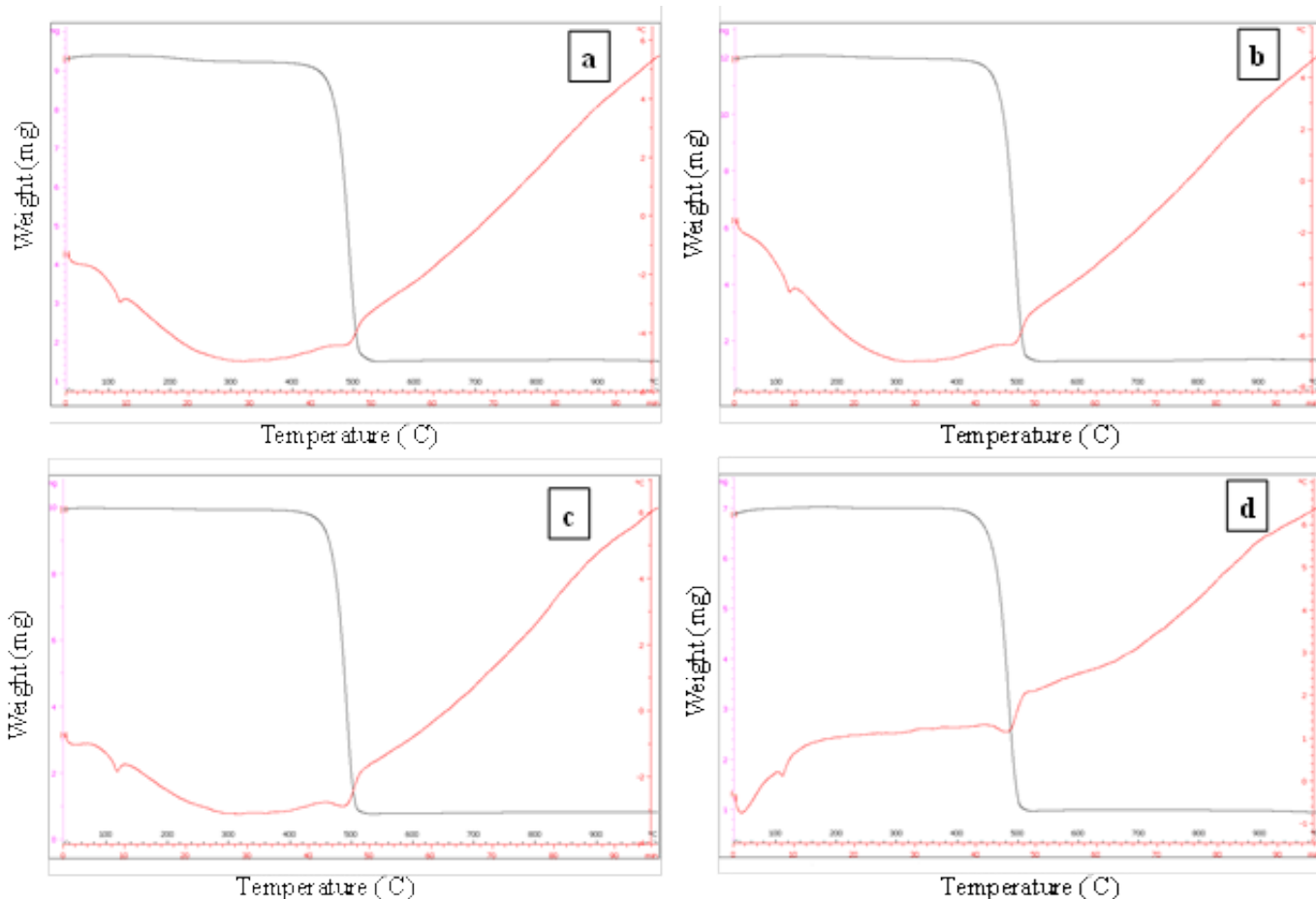


**Figure 6.** TG/DTA curves of LLDPE film and roto grade PPCF (a) LLDPEF 2.2; (b) LLDPEF 2.3; (c) LLDPEF 3.2 and (d) LLDPER 2.2.

**Figure 6** represents the weight loss characteristics as a function of temperature. All of these films display similar thermogram with three distinct weight loss stages centred around 110 °C, 350 °C and 515 °C respectively. The important degradation zones of each film are listed in **Table 5**.

**Table 5.** Decomposition characteristics of LLDPE film and Roto grade PPCF.

Sample code	T peak ( °C)	Mass loss (%)
LLDPEF 2.2	515	80.5
LLDPEF 2.3	515	85.8
LLDPEF 3.2	515	92.1
LLDPER 2.2	500	85.8

At the beginning within the temperature range (100-220 °C), the first weight loss accounts for less than 0.5% is shown which may be due to the removal of moisture or dehydration of phenol (B.P=181.7 °C) from the sample [45]. Similarly, the second weight-loss region with nearly 1.5% weight loss is shown within the temperature range (300-380 °C) may be because of devolatilization of activated carbon [46]. However, the third weight-loss region is centred around (500-515 °C) has been attributed to complete thermal degradation of the polyethylene backbone. With the increase in filler (AC) wt%, there is a decrease in thermal stability in LLDPE PPCF of film grade, however for roto grade with 5% filler addition; the amount of weight loss is comparable to film grade of 10 wt%, which signifies the unsuitability of the roto grade towards film making, for which it was found to be unsuitable for gas separation application [47]. In order to depict more on TGA data, the kinetics of each weight loss process was evaluated by Broido integral method [48]. The rate of change of any chemical thermodynamic processes is expressed as reaction kinetics

$$\frac{dz}{dt} = f(z)^n k(T) \tag{2}$$

Where z is the transmogrification rate depends upon the absolute temperature T. n is the order of reaction. The transmogrification rate or reacted fraction is articulated as the ratio of change in weight loss at distinct time t to the weight loss at an infinite time or total weight loss. The constant is expressed as

$$z = \frac{m_0 - m}{m_0 - m_\infty} \tag{3}$$

Where  $m_0$ , m, and  $m_\infty$  are the sample weight initially, at time t and at the infinite time respectively. As the transmogrification rate is temperature dependent, so it is unique for each elemental weight loss step.

So the rate of reaction can be express in the form of Arrhenius equation.

$$k(T) = A \exp \frac{-E}{RT} \tag{4}$$

Where A is the pre-exponential factor, E is the activation energy and R is the gas constant.

After substitution of eq. (1) in eq. (3) and eq. (2) in eq. (4), the expressions can be rewritten as follows

$$\frac{dz}{f(z)^n} = f(z)^n k(T) \tag{5}$$

$$\frac{dz}{f(z)^n} = k(T) dt \tag{6}$$

$$\frac{dz}{f(z)^n} = A \exp \left( \frac{-E}{RT} \right) dt \tag{7}$$

The first order reaction follows the initial condition of  $z=0$  at  $T=T_0$  which can be expressed in integral form as

$$\int \frac{dz}{f(z)^n} = \frac{A}{\alpha} \int_{T_0}^T \exp \left( \frac{-E}{RT} \right) dt \tag{8}$$

Where  $\alpha$  is the heating rate used in TGA experiment. The simplified expression proposed by Broido might be sufficient to epitomize the membranes weight loss stages in terms of Activation energy.

$$\ln \left[ \ln \left( \frac{1}{y} \right) \right] = \frac{-E}{RT} + constant \tag{9}$$

Where 'y' is the residual fraction can be calculated as

$$y = 1 - z = \frac{m - m_\infty}{m_0 - m_\infty} \tag{10}$$

The plot of  $\left\{ \ln \left[ \ln \left( \frac{1}{y} \right) \right] \right\}$  versus inverse temperature (1/T) obtained from eq. (9) gives a straight line for each step. Hence activation energy can be found out from the slope of the straight line. The unit of the attributes in the given empirical formula are supported to SI. The degradation of the PPCF shows first order kinetics, which is well agreement with other researchers [49,50]. As the process shows maximum degradation in the temperature region of 500-515 °C, so that region became an area of interest for comparative analysis of activation energy. The activation energy calculation for each samples are listed in **Table 6**. The activation energy decreases with increasing filler concentration. As expected highest activation energies are found in LLDPER 2.2, whereas in case of LLDPEF activation energy dramatically decreases due to blend of activated carbon. The presence of secondary phase leads to decrease in thermal stability of the polymer films as well as decrease in activation energy in comparison to virgin polymer. Since LLDEF2.2 shows comparative activation energy and higher thermal stability as compared to other polymeric PPCF, hence it is suitable for high temperature application. The enrich porosity approximately 48% in our study is quite high and comparable to other researchers. As an example, Knapen et al. [51] studied the sound absorption properties of porous mortar with 40% porosity. He reported that such porosity is quite enough for reduction of sound propagation in interior spaces or to improve the control of outdoor noise propagation by use of this mortar as sound absorbing screens. Arena et al. [31] reported the diameter of the perforation should be uniform and less than 0.3 mm for the better results. So from the researchers experimental evidence,

It is quite clear that the synthesised PPCF bearing enrich porosity and high thermal stability which can effectively use as micro perforated panels for sound absorbing materials for various indoor applications.

**Table 6.** Activation Energies calculation of LLDPE film and roto grade PPCF with Broido Integral Method.

Sample code	Activation Energy (kJmol <sup>-1</sup> )
LLDPEF 2.2	45.03
LLDPEF 2.3	44.23
LLDPEF 3.2	43.12
LLDPER 2.2	45.82

## CONCLUSIONS

A facile simple ultra-sonication technique is used for achieving uniform filler dispersion and pore creation. Due to cavitation, bigger pore diminishes and new continuous smaller pore generates. The mean pore diameter of LLDPEF 2.2. and LLDPEF 2.2. decreased from 0.26  $\mu\text{m}$  to 0.15  $\mu\text{m}$  and 1.02  $\mu\text{m}$  to 0.54  $\mu\text{m}$  with 48.5% and 13.84% enhancement in porosity respectively. Among all PPCF, LLDPEF 2.2 (5 wt% filler addition) reproduces better results due to its lower molecular weight. With the increase in filler (AC) wt%, there is a decrease in thermal stability and activation energy in LLDPE PPCF of film grade. Ultimately the study shows lucid evidence for the unsuitability of roto grade LLDPE for film making due to its in-concatenation. These fabricated PPCF can be effectively use as micro-perforated sound absorption panel due to its high porosity. The effect of temperature on pore formation and size selective application is out of scope at this time. Further research should be done to explore the application of ultrasound impulsion to template the pore geometry of porous polymer composite membrane for various filtrations, separation and sound absorbing applications.

## ACKNOWLEDGEMENTS

The authors acknowledge the Ministry of Environment and Forest (MOEF), Govt. of India for its financial support with sanction letter no 19-17/2008-RE.

## REFERENCES

- Dai Z, et al. Honeycomb-like periodic porous LaFeO<sub>3</sub> thin film chemiresistors with enhanced gas-sensing performances. *ACS Appl Mater Interfaces* 2014;6:16217-16226.
- Tuller M, et al. Adsorption and capillary condensation in porous media: Liquid retention and interfacial configurations in angular pores. *Water Resour Res* 1999;35:1949-1964.
- Liu G, et al. Diblock Thin Films with Densely Hexagonally Packed Nanochannels. *J Adv Mater* 1998;10:69-71.
- Khan S, et al. Synthesis and characterization of acrylic resin/activated carbon composites. *IJAP* 2014;52:251-254.
- Ding W, et al. Direct Observation of Polymer Sheathing in Carbon Nanotube-Polycarbonate Composites. *Nano Lett* 2003;3:1593-1597.
- Ferrer PR, et al. Nanostructured porous graphene and its composites for energy storage applications. *Nano Convergence* 2017;4:1-19.
- Lovell CS, et al. Thermodynamic approach to enhanced dispersion and physical properties in a carbon nanotube/polypeptide nanocomposite. *Polymer* 2009;50:1925-1932.
- Teng Y, et al. Conductive Polymer Porous Film with Tunable Wettability and Adhesion. *Materials* 2015;8:1817-1830.
- McCool BA, et al. Synthesis and characterization of mesoporous silica membranes via dip-coating and hydrothermal deposition techniques. *J Memb Sci* 2003;218:55-67.
- Melgar VM, et al. Direct spraying approach for synthesis of ZIF-7 membranes by electrospray deposition. *J Memb Sci* 2014;459:190-196.
- Srinivasarao M, et al. Three-dimensionally ordered array of air bubbles in a polymer film. *Science* 2001;292:79-83.
- Ham HT, et al. Macroporous Polymer Thin Film Prepared from Temporarily Stabilized Water-in-Oil Emulsion. *J Phys Chem B* 2006;110:13959-13964.
- Kuo CY, et al. A Facile Route to Create Surface Porous Polymer Films via Phase Separation for Antireflection Applications. *ACS Appl Mater Interfaces* 2009;1:72-75.
- Morita M, et al. Effects of Applied Potentials on Permselectivity of Ions through Polypyrrole/Porous-Polypropylene Composite Membrane. *J Appl Polym Sci* 1998;70:647-653.

15. Müller K, et al. Review on the Processing and Properties of Polymer Nanocomposites and Nanocoatings and Their Applications in the Packaging, Automotive and Solar Energy Fields. *Nanomaterials* 2017;7:2-47.
16. Wang W, et al. Polymer Composites Reinforced by Nanotubes as Scaffolds for Tissue Engineering. *Int J Polym Sci* 2014;2014:1-14.
17. Huang YY, et al. Dispersion of Carbon Nanotubes: Mixing, Sonication, Stabilization, and Composite Properties. *Polymers* 2012;4:275-295.
18. Li L, et al. Preparation of a Porous Conducting Polymer Film by Electrochemical Synthesis-Solvent Extraction Method. *J Appl Polym Sci* 2004;9:303-307.
19. Padhi P, et al. A Novel Route for Development of Bulk Al/SiC Metal Matrix Nanocomposites. *J Nanotechnol* 2011;2011:1-5.
20. Thomas S, et al. *Rheology and Processing of Polymer Nanocomposites*. 1<sup>st</sup> edition, John Wiley & Sons, Inc. Hoboken, New Jersey 2016.
21. Yang Y, et al. Study on bulk aluminum matrix nano-composite fabricated by ultrasonic dispersion of nanosized SiC particles in molten aluminum alloy. *Mater Sci Eng A* 2004;386: 284-290.
22. Xia HS, et al. Preparation of conductive polyaniline/nanosilica particle composites through ultrasonic irradiation. *J Appl Polym Sci* 2003;87:1811-1817.
23. Kumar S, et al. Fibers from polypropylene/nano carbon fiber composites. *Polymer* 2002; 43:1701-1703.
24. Kruus P, et al. Polymerization resulting from ultrasonic cavitation. *Ultrasonics* 1983; 21:201-204.
25. Kruus P, et al. Polymerization and depolymerization by ultrasound. *Ultrasonics* 1988; 26:352-358.
26. Masselin I, et al. Effect of sonication on polymeric membranes. *J Membr Sci* 2001;181:213-220.
27. Chai X, et al. Ultrasound effect on cross-flow filtration of polyacrylonitrile ultrafiltration membranes. *J Memb Sci* 1998;148:129-135.
28. Lee SH, et al. Three-Dimensional Self-Assembly of Graphene Oxide Platelets into Mechanically Flexible Macroporous Carbon Films. *Angew Chem Int Ed* 2010;49:10084-10088.
29. Overvelde JT, et al. Compaction Through Buckling in 2D Periodic, Soft and Porous Structures: Effect of Pore Shape. *Adv Mater* 2012;24:2337-2342.
30. Kuczmarski MA, et al. *Acoustic Absorption in Porous Materials - NASA Technical Reports*.
31. Chen S et al. The Effects of Various Additive Components on the Sound Absorption Performances of Polyurethane Foams. *Adv Mater Sci Eng* 2015;2015:1-9.
32. Zhang C et al. Correlation between the acoustic and porous cell morphology of polyurethane foam: effect of interconnected porosity. *Mater Des* 2012;41:319-325.
33. Yang X, et al. Sound performance of multilayered composites. *Mater Manuf Process* 2007;22:721-725
34. Arenas JP, et al. Recent trends in porous sound-absorbing materials. *J Sound Vibr* 2010; 44:12-18.
35. Sakagami K, et al. Application of Microperforated Panel Absorbers to Room Interior Surfaces. *IJAV* 2008;13:120-124.
36. Franco F, et al. The effect of ultrasound on the particle size and structural disorder of a well-ordered kaolinite. *J Colloid Interface Sci* 2004;274:107-117.
37. Masselin I, et al. Effect of sonication on polymeric membranes. *J Memb Sci* 2001;181:213-220.
38. Rezvantlab H, et al. An Aqueous-Based Approach for Fabrication of PVDF/MWCNT Porous Composites *Sci Rep* 2017;7:1-10.
39. Dinh TV. *Biomedical Photonics Handbook*, CRC press New work 2003.
40. Padhi P, et al. Effect of modification of zeolite A using sodium carboxymethyl cellulose (CMC). *Bulg Chem Commun* 2014;46:777-783.
41. Rout SK, et al. Effect of modification of Zeolite A using Poly Vinyl Alcohol (PVA). *Bulg Chem Commun* 2016;48:779-786.
42. Zamri MF et al. Improved electrical conductivity of polyvinyl alcohol/ multiwalled carbon nanotube nanofibre composite films with MnO<sub>2</sub> as filler synthesised using the electro spinning process. *IJET* 2011;11:15-21.
43. Abbasi PM et al. Porous carbon nanotube/PMMA conductive composites as a sensitive layer in vapor sensors. *Smart Mater Struct* 2011;20:1-8.
44. Chen R, et al. *Analysis of Thermally Stimulated Processes*. Pergamon, Oxford, (1968).
45. Wang Y, et al. TGA and Time-Dependent FTIR Study of Dehydrating Nafion-Na Membrane. *Macromolecules* 2003;36:1138-1146.

DOI: 10.4172/2321-6212.1000216

46. Kumar S, et al. Integrated Waste Management, In Tech, Chapters 1 2011.
47. Khandanlou R, et al. Mechanical and Thermal Stability Properties of Modified Rice Straw Fiber Blend with Polycaprolactone Composite. *J Nanomater* 2014;2014:1-9.
48. Broido A, et al. A Simple, Sensitive Graphical Method of Treating Thermogravimetric Analysis Data. *J Polym Sci A-2* 1969; 27:1761-1773.
49. Rodrigo L, et al. Thermal analysis of high-density polyethylene and low density polyethylene with enhanced biodegradability. *J Appl Polym Sci* 2002;86:764-772.
50. Westerhout R, et al. Kinetics of the Low-Temperature Pyrolysis of Polyethylene, Polypropene, and Polystyrene Modeling, Experimental Determination, and Comparison with Literature Models and Data. *Ind Eng Chem Res* 1997;36:1955-1964.
51. Knapen E, et al. Acoustic properties of sound absorbing, polymer-modified porous cement mortars. 6th International Conference on Materials Science and Restoration, MSR-VI Aedificatio Publishers 2003; 347-358.